doi:10.1038/nature11734

1 Data

We use the images of the recently concluded S-band Polarization All Sky Survey (S-PASS) that has mapped the polarized radio emission of the entire southern sky with the Parkes Radio Telescope at a frequency of 2307 MHz, with 184 MHz bandwidth, and 9' angular resolution[7]. See Table S1 for a description of the flux densities from the various objects we identify in the main text. For historical interest, Parkes telescope investigations of the Galactic Centre (GC) – and even the discovery of a potential outflow from this region – date back some half a century[30].

1.1 Inference of total intensity flux densities at 2.3 GHz

Confusion with Galactic foregrounds, especially free–free and HII regions, means that we cannot directly measure the total intensity flux density of the Lobes for $|b| \lesssim 15^\circ$. We follow the following procedure to circumvent this problem and estimate the total intensity flux density of the whole Lobes:

1. We measure the integrated polarized intensity of both (whole) Lobes (emission within the edges).

structure name	solid angle [deg^2]	angular width [deg]	2.3 GHz pol. flux density [Jy]	pol. frac.	2.3 GHz total flux density [Jy]
S-PASS Lobes					
north	1751		2610 ± 100	0.25 ± 0.02	10440 ± 450
south	2009		2780 ± 110	0.26 ± 0.02	10690 ± 450
total	3760		5390 ± 150	0.26 ± 0.02	21130 ± 720
Northern Ridge	51.8	2.75	174 ± 14	0.31 ± 0.06	560 ± 110
GC Spur	50.5	1.9	236 ± 8	0.25 ± 0.03	960 ± 132
Southern Ridge	117.6	3.0	373 ± 35	0.31 ± 0.04	1215 ± 130

Table S1: Observed quantities

2. We measure the integrated total and polarized intensity from both Lobes at all latitudes $|b| > 15^\circ$ where the free-free emission is marginal compared to the synchrotron at this frequency.

3. On the basis of these measurements we infer the intrinsic polarization fraction of the synchrotron emission from the Lobes. This is done on the area mentioned above ($|b| > 15^\circ$), that is about 63% of the whole solid angle covered by the Lobes.

4. Assuming the same intrinsic polarization fraction, we infer the integrated, total intensity flux density from the remaining 37% of the Lobes that we cannot measure directly.

1.2 Minimum distance to Lobes from (de)polarization phenomenology

Neither the γ-ray nor the microwave data[1] allow us to infer the distance to the Lobes, but the 2.3 GHz S-PASS data show depolarization at low latitudes around the Galactic Plane that is very informative in this context. S-PASS linear polarized emission and Stokes Q and U images reveal two strong depolarization areas on either side of the Galactic Centre encompassed by a border of small scale modulated signal that extends up to some $|b| \simeq 10^{\circ}$. Both are generated by Faraday Rotation effects generating depolarization (the former) and polarization angle modulation that generates small scale mixing of Stokes Q and U without significant depolarization (the latter). By pinning down the objects responsible for this depolarization we can infer a lower limit on the distance to the Lobes.

Figure S1 shows a comparison between S-PASS Stokes Q (left panel) and the H-α emission as seen in the SHASSA[28] map (right panel). The S-PASS image reveals a number of circular, arc, and bow features in the depolarization regions that match the H-alpha emission regions in SHASSA maps well. We investigated these associations to identify the individual H-α regions and found that most belong to the Sagittarius arm. Moreover, some regions of the more distant Scutum-Centaurus arm are evident emerging behind the Sagittarius arm, like the Scutum super–shell, generating depolarization as well. A few examples of these regions are: G4.28+0.55, G6.09-1.29, G17.4–4.55, G355.05+0.04, G347.70+1.90, G345.00+1.70. Thus, the H-α regions responsible for the depolarization are not objects in the local arm but are located at least 1.5–2.5 kpc from us. Depolarization against the Scutum-Centaurus arm occurs at 3.0-4.0 kpc from us.

The Faraday modulated region surrounding these two areas of depolarization corresponds to weaker H-α enclosing the same group of H-α regions and must be associated with the same spiral arms.

The large scale emission must come from the background of the depolarizing objects. The Lobes' front sides, then, must sit at least at 2.5 kpc from us if we conservatively only account for depolarization by the Sagittarius arm objects. The transverse dimension of the lobes is some 50°, so that, assuming a cylindrical geometry, its centre has to be at least at 4.0 kpc from us and its far side at 5.5 kpc. This is already in the bulge region.

In summary, the S-PASS data implies that the lobes must be located at least as distant as the rim of the Galactic Bulge, in the direction of the Galactic Centre, and huge (extending at least 4.0-5.0 kpc both north and south of the Galactic Plane, implying a minimum total vertical extent of 8.0-10.0 kpc).

[1]Evidence that a distinct, extended, thermal X-ray source – containing close to 10^{56} erg thermal energy – seen in the direction of the Galactic Centre is actually located in its physical vicinity has previously been claimed[29].

2 Equipartition magnetic field calculation

2.1 Equipartition magnetic field calculation for entire structures

We assume that the average path length through the Lobes is 5 kpc and examine two limiting cases: i) synchrotron emission occurs through the entire volume of the Lobes in which case their 21 kJy flux density implies a 6 μG equipartition[11] field as reported; ii) the synchrotron emission occurs in an ensheathing region of 300 pc thickness (the approximate width of the Ridges) with a highly but not perfectly regular field structure. Such a layer would have an equipartition field of 12 μG. Note that, given the rather high polarization fraction at 2.3 GHz, limiting case i) is likely to be somewhat in tension with the inference[31,32] that – given a lack of observed polarized microwave emission coincident with the WMAP 'haze'[33] (see §3) – the interior, volume-filling field structure is highly turbulent (though see ref. [34]). Calculated equipartition magnetic field amplitudes (and the lower and upper magnetic field amplitude limits determined below) for the Lobes and for the Ridges are reported systematically in Table S2 (and consequent magnetic energy densities, total energies, inferred magnetic energy injection rates are presented in Table S3); the Ridges are remarkably similar in their gross characteristics despite their different ages. For the magnetic field energy of the entire structures (in the volume filling field scenario) we assume a total volume of 2×10^{67} cm^3; the modelled, 300 pc-thick sheath has volume 1×10^{66} cm^3.

structure name	assumed distance [pc]	physical width [pc]	height top [pc]	vertical extent [pc]	assumed l.o.s. pathlength [pc]	B_{eq}[⋆] [μG]	B_{BBnd}[†] [μG]	B_{max}[‡] [μG]
S-PASS Lobes volume -filling					5 000	6 $[\alpha^{23}_{2.3} = 1.15]$	>9 $[\alpha^{33}_{23} = -0.7]$	$B^{vol}_{\|\|}$ <25 $B^{vol}_{tot} < 43$[§]
shell only					300	12 $[\alpha^{23}_{2.3} = -1.15]$	>9 $[\alpha^{33}_{23} = -0.7]$	
Northern Ridge	6 000	290	7000	2 100	290	14 $[\alpha^{23}_{2.3} = -1.15]$		
GC Spur	8 000	210	4 000	4 000	270	15 $[\alpha^{23}_{2.3} = -1.01]$	$11 - 18$ $[\alpha^{33}_{23} = -1.25]$	
Southern Ridge	6 000	320	7000	4 900	320	13 $[\alpha^{23}_{2.3} = -1.05]$		

Table S2: **Derived quantities I:** ⋆Equipartition[11] magnetic field. Relative statistical error is 1% from uncertainty in total, 2.3 GHz flux and 6% from uncertainty in 2.3 to 23 GHz spectral index. †Broadband limits on the allowed magnetic field amplitude determined from the consideration that electrons synchrotron radiating at microwave frequencies (and therefore contributing to the WMAP haze emission) will also inverse-Compton radiate into ∼GeV γ-rays (and therefore contribute to the Fermi Bubbles' intensity). Note that the WMAP haze is significantly less extensive in b than the Bubbles or Lobes and that the limit only applies to the solid angle over which it is observed, roughly $b \lesssim 30°$. ‡Derived from tentative detection of polarized, 2.3 GHz emission from rear surface of the outflow and consequent requirement that the change in the polarization angle due to differential Faraday rotation satisfy $\Delta\theta < \pi$ over the 184 MHz bandwidth of the Parkes 2.3 GHz observations. §Derived from $B^{vol}_{||}$ <25 assuming a turbulent magnetic field.

2.1.1 Statistical uncertainties

Formally, the sources of statistical uncertainty in the determination of the equipartition field in the Lobes originate in errors in the measurement of the total flux density from these structures and the 2.3 to 23 GHz spectral index (see Table S1). The 3% relative error on the total flux density from the Lobes implies a partial contribution of 1% to the relative statistical error on B_{eq}. The 9% relative error on the spectral index implies a partial contribution of 6% to the relative statistical error on B_{eq}.

2.1.2 Systematic uncertainties

The systematic error on B_{eq} is dominated by the uncertainty in $\mathbf{K}_0$, the proton-to-electron number density ratio. We choose the theoretically-motivated[35] and observationally-suggested (from local cosmic ray measurements[36]) value of 100 for this parameter. It is to be admitted, however, that, in the unusual environment of the Lobes and Ridges, we cannot be certain this value holds. Still, the dependence of B_{eq} on $\mathbf{K}_0$ is rather weak so that even variation of this parameter by fully an order of magnitude leads to only a $\sim 60\%$ change in B_{eq} (e.g., we have, for the volume-filling field $B_{eq} = \{4, 6, 10\}$ for $\mathbf{K}_0 = \{10, 100, 1000\}$). Moreover, given the timescale requisite to transport the cosmic rays from the plane and the much longer cooling times[5] of cosmic ray ions than electrons in the environment of the Lobes, we expect that – if anything – $\mathbf{K}_0 = 100$ is likely to be underestimate, implying that, conservatively, the equipartition magnetic field we estimate is likely to be lower than the real field. Finally, on the question of whether the physical circumstances in the Lobes and Ridges are such that equipartition actually holds or is, at least, a reasonable approximation, we explain immediately below how an analysis of the broadband data covering the Lobes and the GC Spur implies lower limits to the real magnetic fields in these structures approaching the equipartition magnetic field values we obtain.

3 Broadband phenomenology

At lower Galactic latitudes the Fermi Bubbles – and the Lobes – are coincident with a non-thermal microwave 'haze' found in total intensity WMAP 20-60 GHz data[34,37] of luminosity $(1 - 5) \times 10^{36}$ erg/s (cf. the 1-100 GeV luminosity of the Bubbles of 2×10^{37} erg/s[3]) and their edges are coincident with an hourglass-shaped X-ray structure seen at lower Galactic latitudes in ROSAT data[29] (and attributed to an outflow driven by Galactic centre star formation[12] and also clearly evident in the Stokes U parameter map at 23 GHz (see Figure S3). There are intriguing similarities and differences between emission seen in different wavebands.

We find regions of emission coincident with the 2.3 GHz map not only in the microwaves but also in X-rays (Figure S2) and in γ-rays (Figure 2, main text). In the south west, a spur of X-ray emission appears to wrap around the edge of the southern Fermi Bubble, paralleling but not exactly coincident with the Southern Ridge; this indicates this feature is not simply a limb-brightening in the cone of outflowing plasma (a γ-ray

feature coincident with the Southern Ridge and appearing to 'wrap' in the same fashion is also evident: see Figure 2 of the main text). Coincident, non-thermal emission in 2.3 GHz and 23 GHz polarization and $\sim$GeV γ-rays is evident in the GC Spur, the Southern Ridge, and, indeed, over almost the entire extent of the Bubbles. This indicates a non-thermal electron population covering at least the energy range $\sim$(1-100) GeV (Figure 2, main text) that is simultaneously synchrotron radiating into radio/microwave frequencies and up-scattering ambient light into γ-rays via the inverse Compton process[2].

We find, however, that the broadband data cannot be explained with a single power-law electron population: the spectrum between 2.3 and 23 GHz is considerably steeper ($\alpha \lesssim -1.0$ for $F_\nu \propto \nu^\alpha$) than the very hard spectrum ($-0.4 > \alpha > -0.7$) found[3,4] over 23 to 41 GHz for the haze[3]. Moreover, polarized 2.3 GHz emission is observed considerably outside the γ-ray-defined edges of the Bubbles at high Galactic latitudes (and towards Galactic west). These considerations indicate that a second, high-energy and very hard electron population is either locally accelerated (perhaps powered by magnetic field reconnection) or injected as secondaries (from collisions between cosmic ray protons and the Bubbles' low-density thermal plasma[5] in situ. This is consistent with the fact that the cooling time of the high-energy electrons required to generate the γ-rays is too short for these particles to be transported from the plane out to the full extension of the Bubbles/Lobes given the speed of the outflow (Figure 4, main text).

3.1 Spectral index between 2.3 and 23 GHz polarized emission

The spectral index between polarized emission at 2.3 GHz measured by S-PASS and at 23 GHz measured by WMAP is shown in Figure S4. S-PASS and WMAP polarization maps have been binned to $2^\circ \times 2^\circ$ pixels to improve the signal–to–noise ratio of the 23 GHz data. Noise debiasing has been applied before measurement of the spectral index. As stated in the main text, there is a clear tendency for the spectrum of synchrotron radiation to steepen with distance from the plane (the very flat spectrum in the the plane itself is a spurious result of Faraday depolarization at 2.3 GHz near the Galactic plane). This is a clear indication for the ageing of the synchrotron-emitting cosmic electrons and consistent with their being transported out from the plane.

3.2 Broandband limits on magnetic field

Broadband considerations allow also us to derive a rough lower bound on the magnetic field intensity throughout the volume of the Lobes/Bubbles: the magnetic field must be strong enough that the in situ

[2]We note that the γ-ray spectrum for the 'jet' feature identified by Su and Finkbeiner[3] and claimed by us to be more-or-less coincident with the GC Spur, is distinct from that of the general Fermi Bubble emission surrounding it. In particular, the jet spectrum is both harder and does not exhibit the same low energy cut-off seen in the general Bubble spectral energy distribution below $\sim$1 GeV. This phenomenology is consistent with the jet γ-rays being largely supplied by inverse Compton emission due to primary electrons advected from the plane while, in contrast, the general Bubble γ-ray emission might largely be supplied by proton-proton collisions[5].

[3]Though note that the spectrum that we determine, on the basis of the WMAP data, for the GC Spur between 23 and 33 GHz is, at $\alpha_{23}^{33} \simeq -1.25$, considerably steeper than that determined for the haze.

electron population (required to generate, via synchrotron emission, the observed non-thermal microwave intensity) must not be so numerous that the inverse Compton emission[4] from the same electrons surpasses the observed γ-ray intensity in the Fermi band ($E_\gamma^2 dN_\gamma/dE_\gamma \simeq 4 \times 10^{-7}$ GeV/cm^2/s/sr at a few GeV following ref. [2]). Such reasoning implies $B \gtrsim 9$ μG field for a hard-spectrum electron population with a 1 eV cm^{-3} photon background to up-scatter and $\gamma_e = 2.4$ (for $dN_e/dE_e \propto E_e^{-\gamma_e}$, the particle spectral index corresponding to the steepest allowed spectral index from analysis of the haze emission, $\alpha_{haze} = -0.7$[31], which generates the most conservative lower limit on the field amplitude), and $B \gtrsim 16$ μG for $\gamma_e = 2.0$ (corresponding to $\alpha_{haze} = -0.5$, the central value of the haze spectral index[31]).

Given the evidence that the coincident γ-ray and microwave emission originates from the same cosmic ray electron population (indeed, from electrons in the same energy range), we may apply similar reasoning to the above to determine rough but robust limits to both the lower and upper allowed field strength in the GC Spur. Adopting the intensity reported[3] for the jet-like γ-ray feature recently claimed in the Fermi data (also $E_\gamma^2 dN_\gamma/dE_\gamma \simeq 4 \times 10^{-7}$ GeV/cm^2/s/sr at a few GeV) which is coincident with the GC Spur (identified at radio continuum and microwave frequencies) at $b \sim 15 - 25^\circ$ and using the spectral index measured by us between the polarized emission at 23 and 33 GHz, $\alpha_{23}^{33} \simeq 1.25$, the polarized surface brightness at 23 GHz (1520 Jy/sr) and assuming the polarization fraction of 0.25 measured at 2.3 GHz also applies at 23 GHz, we derive a Stokes I surface brightness of 6100 Jy/sr and determine a lower limit to the total magnetic field amplitude in the GC Spur of 11 μG. We derive a conservative upper limit on the magnetic field from demanding that the cosmic ray electron population that supplies the inverse Compton γ-ray flux from the GC Spur saturate, via synchrotron emission, the whole total intensity at 23 GHz detected over the GC Spur solid angle, 16100 Jy/sr. This saturation point is attained for an $\sim$18 μG field, implying a rough upper limit to the field at this amplitude. In the case of the GC Spur, these lower and upper limits to the field imply that – if equipartition holds – the proton to electron number ratio, $\mathbf{K}_0$ is in the range 30 - 200.

4 Visibility of emission from rear windings at various wavelengths

Our explanation of the geometry of the Ridges – in particular their curvature to Galactic west – requires that, while they wrap around the entirety of the cones defined by the global outflow, rear-side emission from the Ridges is attenuated with respect to the front side emission (the emission from the putative rear part of each Ridge would curve to Galactic east contrary to observations). This relative attenuation must function at 2.3, 23, and 33 GHz; we find that it cannot, then, be a result of simple Faraday depolarization which, for reasonable parameters of magnetic field intensity, plasma density, and path length through the volume of the Lobes, could not appreciably Faraday rotate the polarization angle at microwave frequencies.

In fact, the relative attenuation of the rear, polarized emission can naturally be explained as a consequence of three simple effects which work equally well at radio continuum and microwave frequencies:

[4] In order to calculate the spectrum and luminosity of inverse Compton radiation we employ the RadiationField class[39] from the GalProp code available at http://galprop.stanford.edu/code.php. RMC thanks Troy Porter for assistance with using GalProp's Galactic interstellar radiation field data.

1. The synchrotron intensity scales approximately as B_{perp}^2, where B_{perp} is the component of the magnetic field perpendicular to the line-of-sight. From simple geometrical considerations (see caption to figure S5) the vertical component of B_{perp} is appreciably less in the rear part of a conical outflow than in the front part. The magnetic field direction, moreover, is largely vertical closer to the plane (figure 3 of the main text).

2. Furthermore, along any particular sightline the rear surface is intersected at a greater physical height from the plane than the front surface. This has the consequence that the electron population on the rear is 'older' (more cooled) than the front population.

3. A further (likely) consequence of the greater physical height of the intersection of any given line of sight with the rear surface (relative to the front surface) is that the local magnetic field amplitude at the rear on this line of sight is relatively attenuated (given that the magnetic field is also injected as 'frozen-in' field lines in the plasma outflowing from the plane and will have had more time to reconnect/relax while ascending to a greater height above the plane).

Figure S5 shows the approximate ratio of front-side to rear-side synchrotron intensity taking these effects into account. It is also important to note that horizontal component of B_{perp} completely disappears at the tangent points of the projected outflow edges.

4.1 Upper limit on volume magnetic field from tentative detection of 2.3 GHz polarized emission from rear surface

Note, however, that a blanket statement that polarized emission from the Ridges on the rear surface of the outflow is invisible from our vantage point does not seem to be correct, though such emission is certainly obscured as discussed in the previous section. A careful examination of the Southern lobe in the 2.3 GHz polarization map (Figure S6 and Figure 1 in the main text) reveals features curving in the opposite sense to the Ridges. A clear ridge–like structure – with possible counterparts at other wavelengths – is a linear depolarization feature running from $(l, b) \sim (350^\circ, -17^\circ)$ to $(9, -32)$ (see Figure S6). A likely explanation of this feature is that it runs almost perpendicular to the Southern Ridge so that the polarization angles of the two structures are perpendicular (the magnetic angle is aligned with the Ridges). In turn, both Stokes Q and U have opposite signs for the two ridges and tend to cancel. An important implication of this explanation for the phenomenology is that – even at the comparatively low frequency of 2.3 GHz – intrinsically polarized emission from the rear surface is not Faraday depolarized by its passage through the magnetised plasma inhabiting the volume of the Southern lobe (rather the three geometrical factors outlined in the previous section are responsible for the attenuation of the rear-side synchrotron emission relative to the front-side). We can use this inference to then place an upper limit on the magnetic field in this region of ~ 43 μG: see Table S2.

5 More robust estimate on plasma outflow speed in ridges

The Galactic Centre Ridge diverges from the projected co-rotating point in a fashion that is consistent with angular momentum being conserved in the outflow and the Galactic Centre Spur being 'wound-up' in the outflow[21]. This same analysis points to an initial ratio between the circulation and vertical velocities of the outflow of $v_{circ}/v_{vert} \sim 0.07$. This generates a more accurate estimation of its ascension speed of $\sim$ 1100 km/s v_{circ}/(80 km/s) where we normalise to an 80 km/s circulation speed in the inner $\sim$100 pc as suggested by recent Herschel observations[13].

6 Global analysis

6.1 Considerations around the far infrared-radio continuum correlation

The 60 micron (infrared) flux density[19] of the inner $\sim$200 pc $\times$ 80 pc region around the Galactic centre – essentially the Nuclear Bulge – is 2 MJy [20]. On the basis of the far infrared-radio continuum correlation[19], this level of far infrared emission should be accompanied by a radio continuum flux density of 20.2 kJy at 1.4 GHz. In dramatic contrast, the detected radio continuum flux from the same region is $\sim$ 1.6 kJy at 1.4 GHz, less than 10% of expectation or around 4σ shy of the correlation[40]. Even integrating the radio continuum flux density out to scales of 800 pc in diameter (thereby encompassing the distinct 'diffuse non-thermal source' identified by LaRosa et al.[41] surrounding the Galactic centre), the detected radio continuum flux reaches only 25% of expectation. As has been argued at length elsewhere[40], the explanation for this phenomenology is that the vast bulk of cosmic ray electrons – accelerated in concert with star formation (and consequent supernova activity) in the Galactic centre region – is advected out of the region before the electrons can lose their energy, radiatively, in situ.

Similarly, the γ-ray luminosity of this same inner region is in significant deficit with respect to the expectation[42] were the hadronic cosmic rays accelerated in the region to lose their energy in situ (via collisions on ambient gas); i.e., the system is very far from a 'calorimeter'. Again, the inference that can be made is that the vast bulk of the hadronic cosmic rays also escape the region on an outflow[40].

Where does this power represented by the escaping cosmic ray ions and electrons go? The γ-ray luminosity of the Fermi Bubbles matches the expectation if supplied by hadronic collisions of the cosmic ray protons and ions leaving the Galactic centre[5,6]. Equally, the S-PASS data allow us to determine that the total radio continuum flux density from the Lobes is 21 kJy at 2.3 GHz or $\nu F_\nu = 4.9 \times 10^{-10}$ erg/cm^2/s; the 20.2 kJy at 1.4 GHz predicted by the correlation corresponds[42] to $\nu F_\nu = 2.3 \times 10^{-10}$ erg/cm^2/s at 2.3 GHz or, the expected 2.3 GHz flux density is 11.2 kJy assuming a spectral index of -1.2 between 1.4 and 2.3 GHz. The observed and predicted total flux densities at 2.3 GHz are, therefore, within a factor 1.9 of each other, corresponding to a quite acceptable difference of $\sim$1.1 σ (adopting the 0.26 dex scatter in the empirical correlation from ref. [19]). Given a number of uncertainties – particularly the effect that the spreading of the outflow cones will mean that the r^2-biased emission from the front of the outflow takes place significantly

closer than the ~ 8 kpc distance to the GC (at which distance the Galactic centre star-formation-related far infrared light is emitted) – we view this level of agreement, as stated in the main text, as a strong argument that the Lobes' non-thermal radio emission is supplied by synchrotron emission from cosmic ray electrons accelerated by star-formation activity in the Galactic Centre.

6.2 Gross Energetics

The current star-formation rate in the inner ~ 100 pc (in radius) region around the GC is slightly below $0.1\ M_\odot$/year (see ref. [6] and references therein). Given the $\sim 10^9\ M_\odot$ mass of the stellar population inhabiting this region (the Nuclear Bulge[20,43]), the current value is close to the time-averaged value over the last ~ 10 Gyr. Using, conservatively, standard assumptions (i.e., the initial mass function, IMF, for the zero-age, main sequence stellar masses is given by a Kroupa[44] IMF with a minimum stellar mass of $0.07\ M_\odot$, the total mechanical energy release per core-collapse supernova is 10^{51} erg irrespective of the progenitor's zero-age, main sequence mass) this star formation rate translates to a mechanical power injection rate from the region's core-collapse supernovae of $\sim 10^{40}$ erg/s[6,15]. By way of comparison, the power requisite to inflate the magnetic fields of the expanding Ridges and supply their cosmic ray content is $\sim 2 \times 10^{39}$ erg/s (see Table S3) assuming that the equipartition approximation holds. These energetics can be satisfied by the mechanical power available from the region's supernovae under the most conservative assumptions.

structure name	volume [cm^3]	$u_{B_{eq}}$ [eV cm^{-3}]	$U_{B_{eq}}$[†] [erg]	age[⋆] [Myr]	t_{exp}[⋆] [Myr]	$\dot{E}_{mag}$[‡] [erg/s]
S-PASS Lobes						
vol.-filling	2.0×10^{67} cm^3	0.8	3×10^{55}	300[§]	300[§]	
shell only	1.2×10^{66} cm^3	3	8×10^{54}	90[§]	90[§]	
northern ridge	5.0×10^{63} cm^3	5	4×10^{52}	4.7	1.4	8×10^{38}
GC Spur	5.2×10^{63} cm^3	4	7×10^{52}	2.8	2.8	8×10^{38}
southern ridge	1.4×10^{64} cm^3	4	9×10^{52}	4.7	3.4	9×10^{38}

Table S3: **Derived quantities II:** ⋆Assumes expansion velocity $v_{exp} \equiv 1400$ km/s. In principle, both the quoted ages and expansion times are lower limits because each Ridge structure disappears around the edge of the general outflow. †Total magnetic energy assuming equipartition. ‡$\dot{E}_{mag} \equiv U_{B_{eq}}/t_{exp}$. §*Assumes* magnetic power injected at a rate 3×10^{39} erg/s.

7 Discussion of thermal X-ray fluxes

From ROSAT X-ray data covering the Lobes[29,38] we find a background-subtracted count rate of 300×10^{-6} cnt/s/arcmin^2 over the R6 band (0.91 - 1.31 keV) for the bright X-ray counterpart to the southern Ridge (see Figure S2). This corresponds to an intensity of $\sim 8 \times 10^{-8}$ erg/cm^2/s/sr. Obviously, this region is atypically bright in comparison to the whole solid angle of the Lobes but we use this intensity in the context of generating various limits. (Also note, given the scale of other uncertainties, we are not correcting for

photoelectric absorption. This we expect to be a reasonably small correction given that we infer from the data presented in ref. [38] an optical depth at $\sim$ keV of ~ 0.4)

We first use this intensity to derive a (somewhat temperature-dependent) upper limit on the plasma density. Assuming a volume-filling plasma of $\sim 3 \times 10^7$ K, we derive from ref.[45], an upper limit on the density of this plasma of $\sim 3 \times 10^{-3}$ cm^{-3}. Assuming, more naturally, that the observed X-rays are generated by plasma entrained in the Southern Ridge outflow, assuming a 300 pc pathlength through this structure, we obtain a plasma density of $\sim 2 \times 10^{-2}$ cm^{-3} for the same assumed temperature (we obtain $\sim 9 \times 10^{-3}$ cm^{-3} for $T = 10^7$ K) which defines an upper limit on the plasma density for the region. For a 1100 km/s outflow, this density then implies a $\sim 2 - 4 \times 10^{-2}\, M_\odot$/year mass flux along the Southern Ridge. Very roughly, this suggests that the mass flux along all of the ridges is $\sim 0.1\, M_\odot$/year, a comfortable fraction of the mass accretion rate on to the GC of $\sim 0.3\, M_\odot$/year (see ref. [6] and references therein).

7.1 Inferred Alfven velocities

Given the upper limit on the plasma density and assuming the equipartition magnetic field amplitude, we may obtain the Alfven velocity, $v_A^2 \equiv B^2/(4\pi m_p n_p)$. The component of this resolved into the vertical direction is $v_A^{vert} \simeq 300$ km/s (for $T \sim 10^7$ K and $B = 15\ \mu$G).

8 Relating Ridges to GC super-stellar clusters

Assuming a reasonable fraction ($\sim$20%) of the typical mechanical energy of a supernova (10^{51} erg) ends up in cosmic ray and magnetic energy, the Ridges each require $400 - 1000$ supernovae or the formation of a total stellar mass of $(3 - 9) \times 10^4\, M_\odot$. This requires the accumulation of $> (0.4 - 1) \times 10^6$ years' star formation given the star-formation rate in the region. Such a timescale and the total stellar mass quoted are comparable to those associated with the formation of the observed massive stellar clusters in the Galactic Centre (e.g., ref. [46]). As we have already noted, the gross energetics of the Ridges can be supplied by core-collapse supernovae occurring with the frequency implied by the Galactic Centre's current star-formation rate.

Note, however, a complicating factor: for any discrete star-formation event there is a delay of ~ 3 Myr (e.g., ref. [47]) between the onset of star-formation and the first core-collapse supernovae (originating in the most massive stars). In the strong tidal fields of the Galactic centre, moreover, stellar clusters are completely disrupted over a timescale ~ 10 Myr[48] or, at least, suffer sufficient dissolution that they become invisible against the high stellar density background within a similar timeframe[49]. In general terms, this means that, whereas the most massive stars of the super-stellar clusters contribute to the outflows forming the Ridges (both in terms of their winds and their supernovae which occur soon enough after cluster formation that the cluster is still coherent), core-collapse supernovae arising in less massive stars are more broadly distributed through the region and would seem to be prime candidates for energising the general bi-conical outflow

feeding into the extended Lobes/Bubbles. Consistent with this picture, the mechanical power injected by the combined stellar winds of a $\sim 5 \times 10^4\ M_\odot$ super-stellar cluster (a reasonable estimate for, e.g. the initial mass of either the Arches or Quintuplet clusters) is at least a few $\times 10^{39}$ erg/s (see, e.g., Figure 1 of ref.[50]), enough to initially supply the Ridges' magnetic fields and cosmic ray content. Likewise, the mass flux along the Southern Ridge represented by the outflowing plasma, $\sim 2-4\times10^{-2}\ M_\odot$/year as derived above, is well accounted-for by mass loss due to massive stellar winds from a similarly-sized cluster (see, e.g., Figure 11 of ref.[50]), allowing for an expected mass-loading of 3-10[51] and further mass injection by supernovae. This mass flux also represents a comfortable fraction ($\sim 10\%$) of the model-derived[6] total plasma mass flux into the entire outflow.

9 Collimation of the Ridges

One significant aspect of the winding's phenomenology is that they remain coherent over many kpc with rather constant widths. Aside from the implication that the windings present a channel to deliver cosmic rays from the Galactic nucleus out into the halo with little adiabatic loss, their collimation likely implies a particular magnetic field topology: a 'force-free' configuration where the toroidal and longitudinal components of the field satisfy $B_\phi \gtrsim B_{||}$ and the magnetic structure is self-confined[52]. Confirmation of this speculation and exactly how such a field configuration is produced is a subject of ongoing investigation.

References

[30] Kerr, F. J., & Sinclair, M. W. A Highly Symmetrical Pattern in the Continuum Emission from the Galactic Centre Region, Nature, 212, 166 (1966)

[31] Dobler, G., & Finkbeiner, D. P., Extended Anomalous Foreground Emission in the WMAP Three-Year Data Astrophys. J., 680, 1222 (2008)

[32] McQuinn, M., & Zaldarriaga, M. Testing the Dark Matter Annihilation Model for the WMAP Haze, Mon. Not. Roy. Astron. Soc., 414, 3577 (2011)

[33] Gold, B., Odegard, N., Weiland, J. L., et al. Seven-year Wilkinson Microwave Anisotropy Probe (WMAP) Observations: Galactic Foreground Emission, Astrophys. J. Supp., 192, 15 (2011)

[34] Dobler, G. A Last Look at the Microwave Haze/Bubbles with WMAP, Astrophys. J., 750, 17 (2012)

[35] Bell, A. R. The acceleration of cosmic ray shock fronts – 1, Mon. Not. Roy. Astron. Soc., 182, 147 (1978)

[36] Ginzburg, V. L., & Ptuskin, V. S. On the origin of cosmic rays: Some problems in high-energy astrophysics, Reviews of Modern Physics, 48, 161 (1976)

[37] Finkbeiner, D. P. Microwave Interstellar Medium Emission Observed by the Wilkinson Microwave Anisotropy Probe, Astrophys. J., 614, 186-193 (2004)

[38] Snowden, S. L., et al. ROSAT Survey Diffuse X-Ray Background Maps. II., Astrophys. J., 485, 125 (1997)

[39] Porter, T. A., Moskalenko, I. V., Strong, A. W., Orlando, E., & Bouchet, L. Inverse Compton Origin of the Hard X-Ray and Soft Gamma-Ray Emission from the Galactic Ridge, Astrophys. J., 682, 400 (2008)

[40] Crocker, R. M., Jones, D. I., Aharonian, F., et al. γ-rays and the far-infrared-radio continuum correlation reveal a powerful Galactic Centre wind, Mon. Not. Roy. Astron. Soc., 411, L11-L15 (2011a)

[41] LaRosa, T. N., Brogan, C. L., Shore, S. N., Lazio, T. J., Kassim, N. E., & Nord, M. E. Evidence of a Weak Galactic Center Magnetic Field from Diffuse Low-Frequency Nonthermal Radio Emission, Astrophys. J., 626, L23 (2005)

[42] Thompson, T. A., Quataert, E., & Waxman, E. Starbursts and Extragalactic γ-ray Background, Astrophys. J., 654, 219 (2007)

[43] Serabyn, E., & Morris, M., Nature, 382, 602 (1996)

[44] Kroupa, P. On the variation of the initial mass function, Mon. Not. Roy. Astron. Soc., 322, 231 (2001)

[45] Raymond, J. C., Cox, D. P., & Smith, B. W., Radiative cooling of a low-density plasma, Astrophys. J., 204, 290 (1976)

[46] Harfst, S., Portegies Zwart, S., & Stolte, A. Reconstructing the Arches cluster - I. Constraining the initial conditions, Mon. Not. Roy. Astron. Soc., 409, 628-638 (2010)

[47] Mo, H., van den Bosch, F. C., & White, S. , Galaxy Formation and Evolution. Cambridge University Press, 2010. ISBN: 9780521857932 (2010)

[48] Kim, S. S., Figer, D. F., Lee, H. M., & Morris, M. N-Body Simulations of Compact Young Clusters near the Galactic Center, Astrophys. J., 545, 301 (2000)

[49] Portegies Zwart, S. F., Makino, J., McMillan, S. L. W., & Hut, P. The Lives and Deaths of Star Clusters near the Galactic Center, Astrophys. J., 565, 265 (2002)

[50] Côté, B., Martel, H., Drissen, L., & Robert, C. Galactic outflows and evolution of the interstellar medium, Mon. Not. Roy. Astron. Soc., 421, 847 (2012)

[51] Strickland, D. K., & Heckman, T. M. Supernova Feedback Efficiency and Mass Loading in the Starburst and Galactic Superwind Exemplar M82, Astrophys. J., 697, 2030 (2009)

[52] Bicknell, G. V., & Li, J. The Snake: A Reconnecting Coil in a Twisted Magnetic Flux Tube, Astrophys. J., 548, L69-L72 (2001)

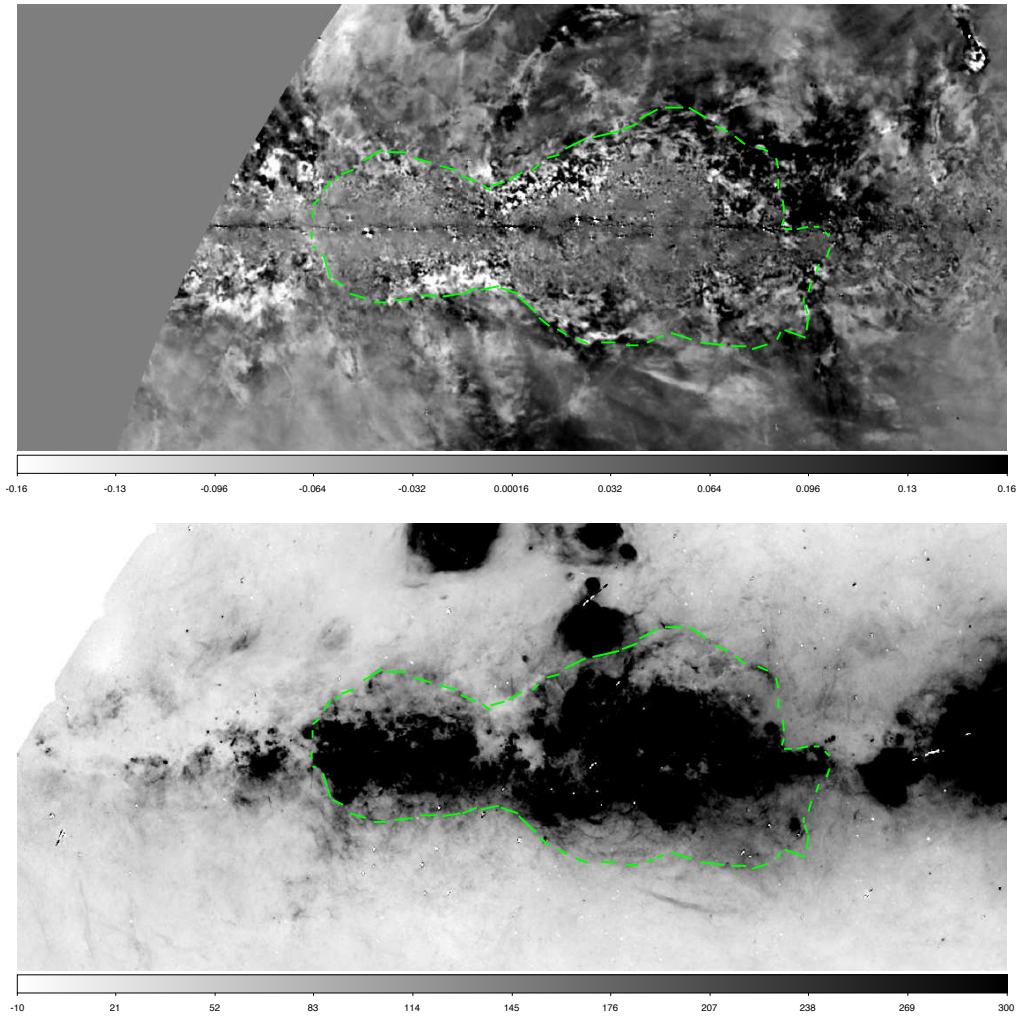

Figure S1: Top: **Stokes Q image of the area around the Galactic Centre.** The Galactic plane is horizontal across the picture and the emission unit is Jy/beam with a beam of FWHM=10.75'. The green dashed line indicates the two areas of depolarization on either side of the Galactic Centre and the belt encompassing them of emission modulated to small angular scales by Faraday Rotation effects. Bottom: **H-α emission image of the same area from the SHASSA survey**. The emission unit is decirayleighs (dR); The resolution is FHWM=6'. The area affected by Faraday Rotation effects is reported as well and corresponds to H-α emission regions from the Sagittarius and Scutum-Centaurus arms – see text.

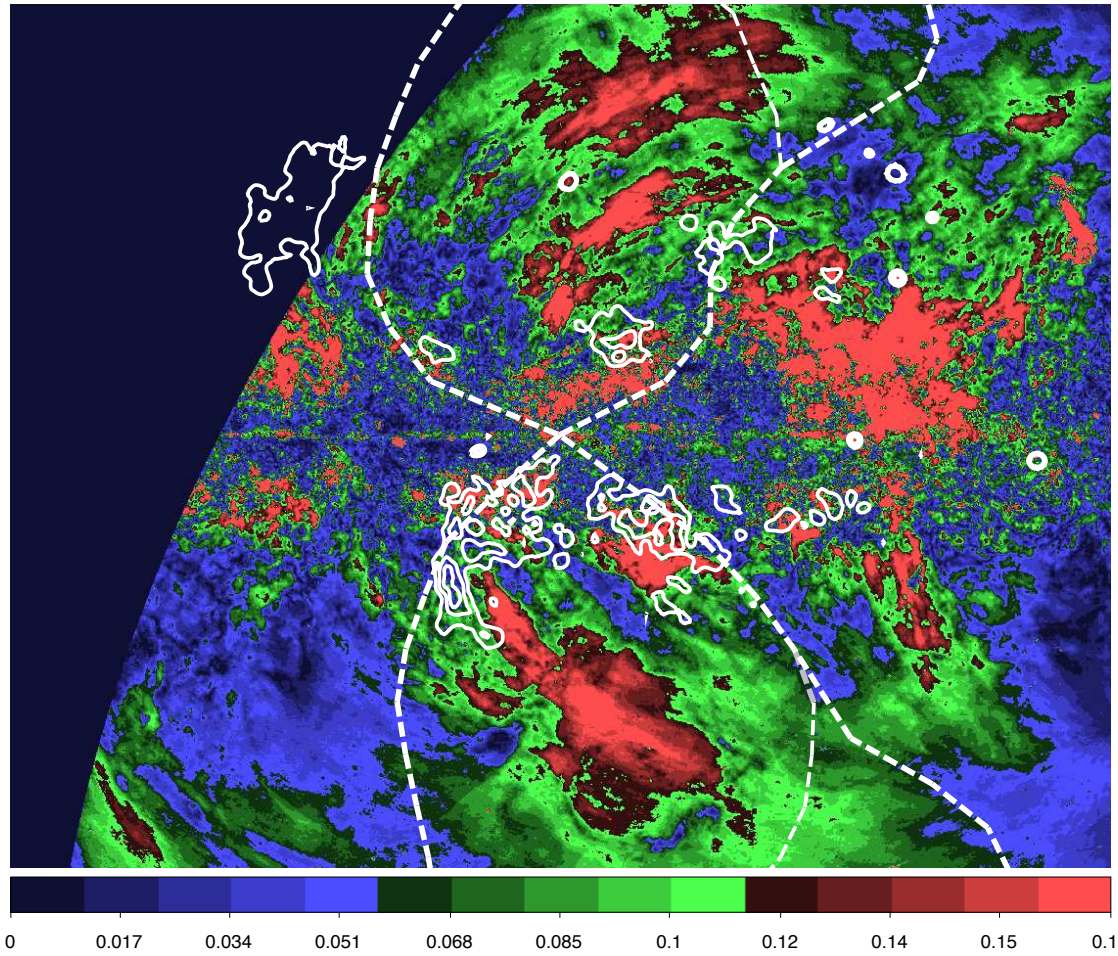

Figure S2: **S-PASS and X-ray emission**. Data are: i) polarized emission from S-PASS shown in colour – unit is Jy/beam); ii) X-ray emission as detected by ROSAT (white contour levels, ranging from 250 to 550×10^{-6}cts/s/arcmin^2 with steps of 75). ROSAT data are the average of the bands 5 and 6 and the band 7 subtracted to remove the large scale emission and emphasise substructures. The thick dashed lines show the edges of the S-PASS Lobes and the thinner dashed lines the edges of the γ–ray Fermi Bubbles as defined by Su et al.[2].

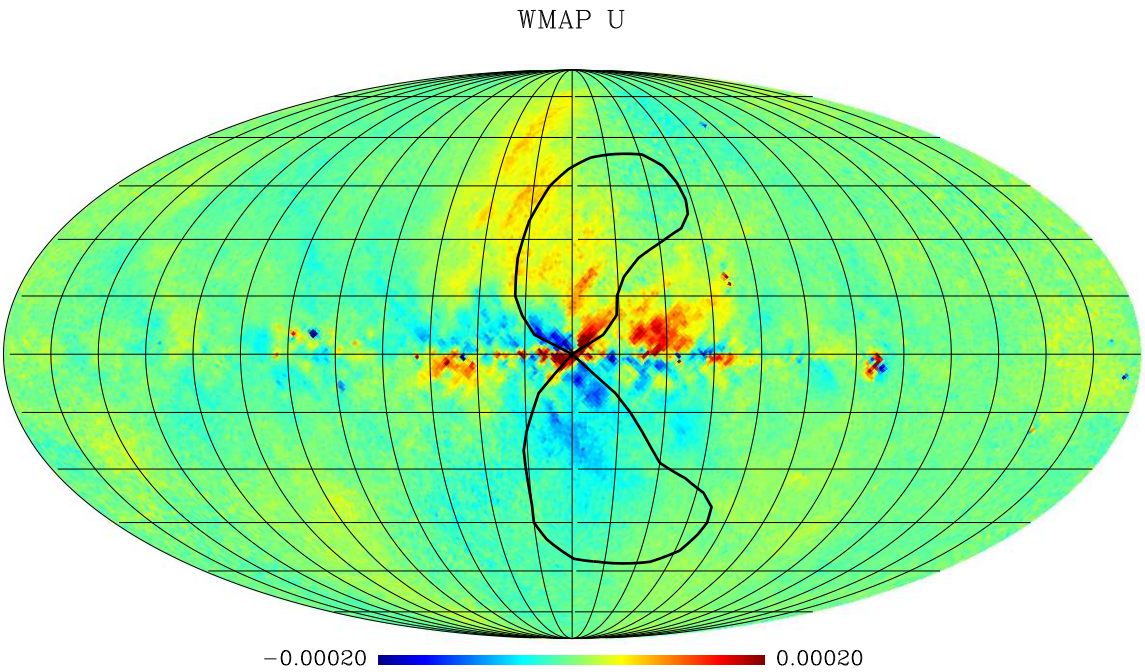

Figure S3: **Linear polarization emission component Stokes U at 23 GHz from WMAP[8].** An X-shape structure centred at the Galactic Centre matches the biconical Lobe base as traced by X-ray emission (cf. Figure 6c of ref. [12] and ref. [38]) and could be limb brightening of the Lobes (the 2.3 GHz Lobe edges shown by the black solid line). Stokes U is less contaminated by spiral arm emission contamination than Stokes Q because the magnetic angle of the arm emission is largely parallel to the Galactic plane[8]. The map is in Galactic coordinates, centred at the Galactic Centre. Grid lines are spaced by 15°. The emission intensity is in Brightness Temperature, the unit is K. Data have been binned in $1^\circ \times 1^\circ$ pixels.

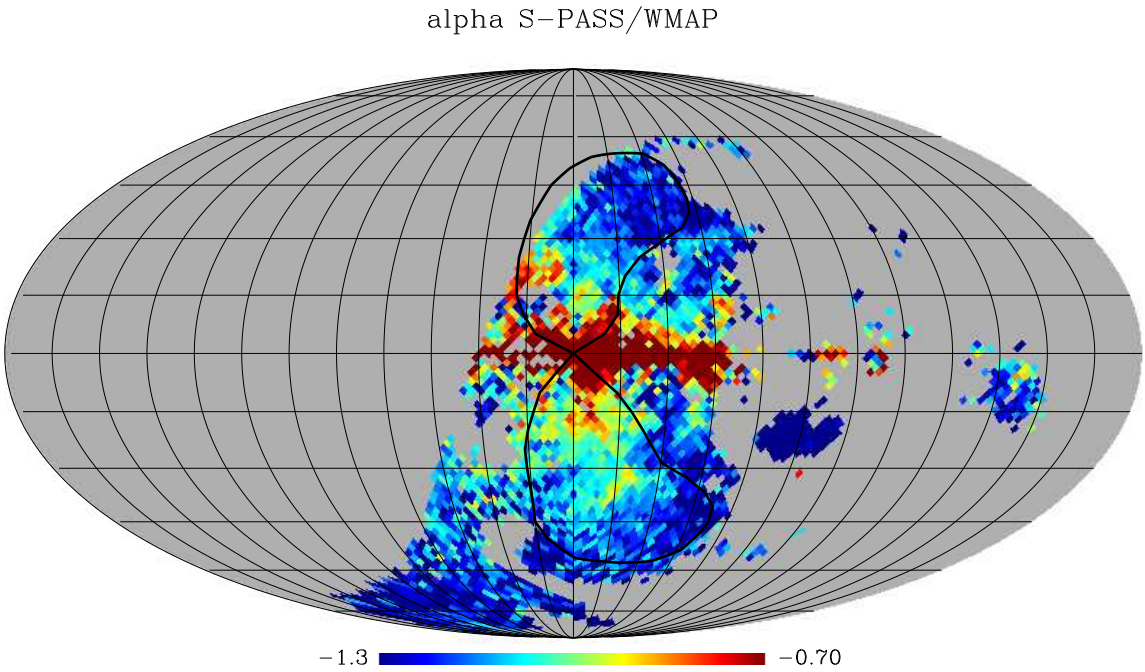

Figure S4: **Spectral index α between the 2.3 and 23 GHz polarized emission.** The flux density S is modelled as a power law of the frequency $S \propto \nu^{\alpha}$. The map is in Galactic coordinates, centred at the Galactic Centre. Grid lines are spaced by $15°$. S-PASS and WMAP linear polarized emission maps have been binned in $2° \times 2°$ pixels to improve the Signal-to-Noise ratio of the latter.

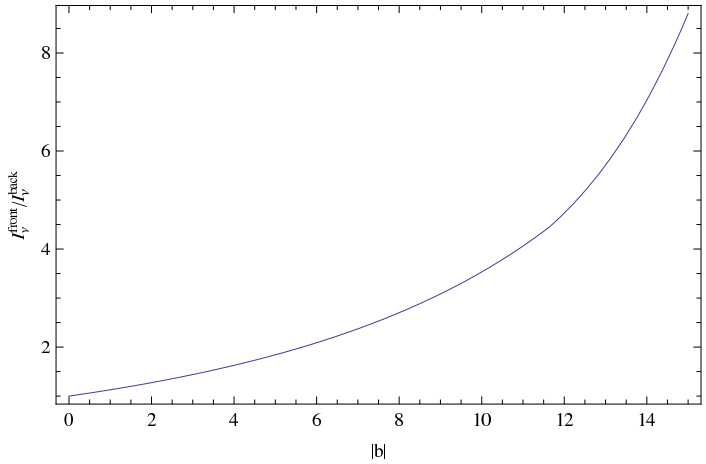

Figure S5: **The approximate ratio of front-side to rear-side synchrotron intensity as a function of Galactic latitude.** The relative attenuation of the rear side synchrotron emission with respect to the front side is a consequence of three geometrical factors: i) (the vertical component of) the magnetic field perpendicular to the line of sight, B_{perp}, is relatively reduced on the rear surface by a factor $\sim \cos(|b| - \alpha)/\cos(|b| + \alpha)$ where b is the latitude and α is the half opening angle of the outflow (the synchrotron intensity scales approximately as B^2_{perp}); the front surface of the outflow intersects a given line of sight (los) at a smaller physical distance from the plane than the rear surface which has the dual effects that ii) the rear surface electrons are relatively older (and therefore more cooled) along any given los and iii) the rear surface magnetic field along the given los might be expected to be relatively attenuated. We can approximately calculate the effects of ii) and iii) together by calculating the ratio of the total intensity along a given los (with given Galactic latitude b) to the intensity along a line of sight at the (higher) latitude b' which corresponds to the angle required such that this new los intersects the $front$ surface at the same physical height above the plane that the original los intersects the $rear$ surface. Note that – consistent with the X-ray observations tracing the edge of the Lobes/Bubbles relatively close to the plane[12] – we set the outflow opening angle to be $\alpha = 60^\circ$ in this plot. The plot also implicitly assumes that the magnetic field orientation is vertical; this is a good approximation over the latitude range of the plot.

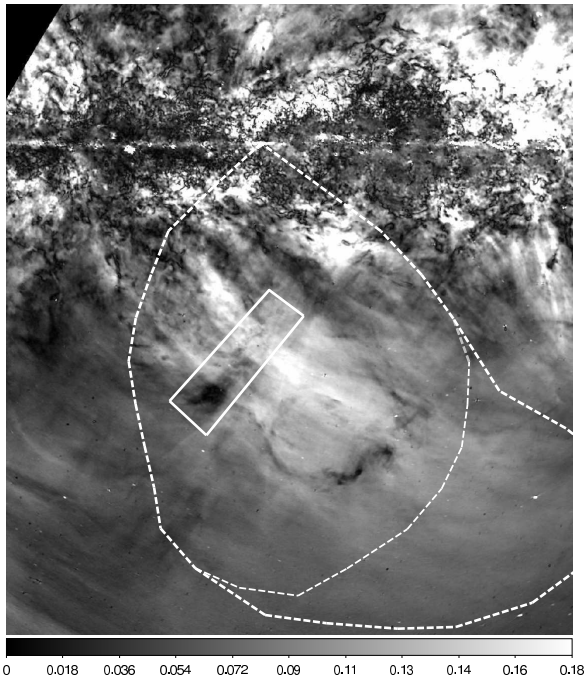

Figure S6: **Black and white image of the polarised intensity at 2.3 GHz.** A suspected rear winding running from $(l, b) \sim (350°, -17°)$ to $(9, -32)$ is visible as a region of relatively *low* intensity (i.e., darker) within the box (white solid line) in the southern S-PASS Lobe. This region is likely dark because the magnetic field direction in a rear winding will be roughly perpendicular to the field in the front surface leading to cancellation of both Stokes U and Stokes Q parameters, hence cancellation of the total polarised intensity along this line of sight.